Climate Dynamics (2001) 18: 241–253

A. Diedhiou · S. Janicot · A. Viltard · P. de Félice

Composite patterns of easterly disturbances over West Africa and the tropical Atlantic: a climatology from the 1979–95 NCEP/NCAR reanalyses

Received: 18 August 1999 / Accepted: 14 March 2001

Abstract The horizontal and vertical structure of the 3–5-day and 6–9-day easterly waves over West Africa and tropical Atlantic are investigated. NCEP/NCAR reanalyses are used for the period 1979–1995 to produce a 17-year climatology of both 3–5-day and 6–9-day easterly waves. Composite patterns of convection, wind, temperature and vertical velocity are analysed with respect to the following: the modulation by 3–5-day and 6–9-day wave regimes; the contrasts between the ITCZ (5°N–10°N) and the Sahelo-Saharan band (15°N–20°N); the difference between land and ocean, and seasonal variations. Similarities and differences in the characteristics of the two wave regimes are identified.

1 Introduction

Easterly waves have been identified as synoptic weather systems, travelling westward, west of 20°E, over West Africa and the tropical Atlantic. They have a wavelength between 1500 km and 4000 km and a speed of about 8 m s^{-1}, giving to periods between 2.5 and 5.5 days.

Composite analysis has previously been used to characterise the horizontal and vertical structure of the 3–5-day easterly waves, but only on small samples: GATE in 1974 with radiosonding data (Burpee 1974, 1975; Reed et al. 1977; Thompson et al. 1979; Chen and Ogura 1982) and the summer of 1985 with European Centre for Medium-range Weather Forecast (ECMWF) analyses (Duvel 1990). In these studies both land (from west coast of Africa to 10°E) and ocean (from 40°W to west coast of Africa) have been considered and different latitudes between 5°N and 20°N have been used as references to compute the composite fields. With a reference latitude located between 11°N and 12°N, Reed et al. (1977) found for the eight wave disturbances of the GATE Phase III (23 August–19 September), a strong modulation of the meridional wind component at 650 hPa, between the equator and 30°N, with a marked southwest-northeast tilt south of the reference latitude. The centre of the composite wave trough is located on the reference latitude and is associated with a cold core below the jet and a warm core above.

At the land surface two circulation centres are evident, one south of the upper centre and possibly of convective origin, and the other 10° to the north at about the latitude of the monsoon trough, relatively cloud-free (Carlson 1969). These two centres merge into one over the ocean because of the southward dip of the monsoon trough and the more northward location of the upper centre steering by the middle-level flow on the southern African Easterly Jet (AEJ) border. Maximum low-level convergence and upward vertical motion, as well as greatest convective cloud cover and largest precipitation amounts, are located in the region ahead and slightly south of the wave trough. However at 20°N the positive rainfall anomalies are located behind the trough between the southerly wind and ridge sectors, indicating the primary influence of northward horizontal transport of moisture (Burpee 1974; Duvel 1990). No vertical tilt is evident south of the AEJ because of the influence of convective heating whereas at 15°N a vertical tilt opposed to the vertical wind shear shows the significant role of dry baroclinic processes in cloud-free areas (Burpee 1974).

Over the ocean wavelengths are shorter, vorticities are greater at all levels, the horizontal wave axis is more tilted at levels close to the AEJ core, and upward vertical motions are weaker in the upper troposphere, suggesting that the convection is not as deep as over land.

A. Diedhiou (✉)
IRD/LTHE, BP 53, 38041,
Grenoble Cedex 9, France
E-mail: diedhiou@hmg.inpg.fr

S. Janicot
METEO-France, D2 C/MAV/MP, 75340,
Paris Cedex 7, France

A. Viltard · P. de Félice
Université Paris XII/LMD (CNRS),
91128, Palaiseau, France

Duvel (1990) investigated the relation between easterly waves and cloudiness in summer 1985 with ECMWF analyses and METEOSAT dataset on four regions, centred on latitudes 7.5°N and 17.5°N, both on land and ocean. His results are in good agreement with those obtained on GATE. In particular, for land and oceanic regions around 7.5°N, the larger deep convective activity at and ahead of the wave trough is well related to the maximum low-level convergence and high-level divergence, upward velocity being stronger at high-levels over land. At latitudes near 17.5°N over the Saharo-Sahelian region, the deep convection has a primary maximum in the southerly wind sector, fuelled by horizontal transport of moisture. At and ahead of the trough axis there is a highly suppressed cloud condition, consistent with a strong shallow dry convection. For oceanic regions near 17.5°N, the maximum cloudiness is in phase with the maximum southerly wind. Duvel (1990) suggested that in the Inter-Tropical Convergence Zone (ITCZ), convection located ahead of the trough may exert a positive feedback on the wave by increasing cyclonic vorticity, whereas over Saharo-Sahelian regions this feedback is quite small and not positive, because the deep convection does not occur in the wave trough.

In recent studies (Diedhiou et al. 1998a, b, 1999, henceforth DJa, DJb, DJc), the mean kinematic characteristics of easterly waves and the associated modulation of convection have been investigated in the long-term reanalysis datasets of NCEP/NCAR (period 1979–1995) and ECMWF (period 1979–1993). In the northern summer, two main periodicities were highlighted by a spectral analysis of the meridional wind component at 700 hPa. They lie between 3 and 5 days and 6 and 9 days. For the 3–5-day easterly wave regime, two main tracks have been identified over West Africa, at 5°N and at 15°N, which merge into one track over the tropical Atlantic along 17.5°N. These waves, most active in August–September, have a mean wavelength and a mean phase speed varying from 3000 km/8 m s^{-1} north of the AEJ to 5000 km/12 m s^{-1} south of the AEJ. Rainfall, convection and the monsoon flux are significantly modulated by these waves, convection in the ITCZ being enhanced in and ahead of the trough. The 6–9-day regime is more intermittent and the corresponding wind field pattern has both similar and contrasting characteristics. There is only one main track, located north of the AEJ along 17.5°N over West Africa and the tropical Atlantic. The mean wavelength is larger, about 5000 km, and the mean phase speed is about 7 m s^{-1}. The perturbation of the wind field is then mostly evident at and north of the AEJ latitude. It leads to a large modulation of the zonal wind component of the jet. These 6–9-day easterly waves also significantly modulate rainfall, convection and the monsoon flux, resulting in zonal convective bands in the ITCZ extending mostly in and behind the trough. This 6–9-day regime appears as an interaction between the 3–5-day regime and strong anticyclonic circulations north of the AEJ.

As part of the West African Monsoon Project (WAMP more information on this 3-year European project (1998–2000) can be found at the web site http://www.met.reading.ac.uk/~swsthcri/tropical.html), our purpose is to investigate further the horizontal and vertical structure of the 3–5-day and 6–9-day easterly waves over land over ocean by using the composite analysis applied by Reed et al. (1977) and others, on NCEP/NCAR reanalyses over the period 1979–1995. This will also enable us to identify better the similar and different characteristics of the 6–9-day easterly wave regime compared to the 3–5-day regime. Composite patterns of convection, wind, temperature and vertical velocity will be analysed with respect to the following: the modulation by 3–5-day and 6–9-day wave regimes; the contrasts between the ITCZ (5°N–10°N) and the Sahelo-Saharan band (15°N–20°N); the difference between land and ocean, and seasonal variations.

We have also used the observed daily rainfall over West Africa from IRD (Institut de Recherche pour le Développement) data base for the period 1979–1990. These daily values have been interpolated in space on the NCEP 2.5° × 2.5° grid by assigning each station daily value to the nearest grid point and averaging all the values related to each grid point. The infrared cloud amounts of C1 dataset from the International Satellite Cloud Climatology Project (ISCCP; Rossow and Schiffer 1991) has also been used in this study over the summers 1984 to 1988, only available for us at this time. Data has been spatially interpolated on the NCEP/NCAR 2.5° grid with a software provided in the ISCCP databank and is available in seven pressure layers (1000–800 hPa, 800–680 hPa, 680–560 hPa, 560–440 hPa, 440–310 hPa, 310–180 hPa and 180–5 hPa).

In the next section, the composite patterns during these two wave regime are presented. Horizontal and vertical composite diagrams, similar to those presented by Burpee (1975), Reed et al. (1977) or Duvel (1990), have been computed over land and ocean, separately for June–July and August–September. A general synthesis is given in Sect. 3. To save space, only August–September results are shown here. June–July results will be discussed only when significant differences exist.

2 Result of composite analysis

2.1 Method

We have applied a composite method close to the method that has been widely used to characterise the horizontal and vertical structure of 3–5-day easterly waves (Reed and Recker 1971; Burpee 1975; Reed et al. 1977; Thompson et al. 1979; Chen and Ogura 1982; Duvel 1990). In this method a pressure level (here 700 hPa) and a latitude where the waves have large amplitudes are chosen as references. The composite is accomplished by dividing each wave into eight categories determined from the filtered time series of a wind parameter (here the meridional wind component) at the reference pressure level and latitude. Based on the results presented in DJc, we have selected three latitudes of reference over the continent and one over the ocean. Over West Africa, we have used the latitudes 5°N and 15°N for the 3–5-day easterly waves, and we have computed the composite over the longitudes 17.5°W to 5°E. We have selected the latitude 17.5°N for the 6–9-day easterly waves,

and we have computed the composites over the longitudes 17.5°W to 30°E. Over the Atlantic, we have used the reference latitude 17.5°N for both the 3–5-day and the 6–9-day easterly waves and we have computed the composites over the longitudes 70°W to 20°W. These latitudes, representing the main tracks of these waves, have not been defined from the location of greatest wind variance, but from the areas where the waves are the best organised (see DJc for more details).

Duvel (1990) discussed the influence of the reference latitude by noting that a composite signal at a given latitude is modulated depending on the reference latitude. We obtained similar conclusions with a sensitivity investigation of the influence of both the latitude and parameter (zonal and meridional wind component) referenced to resulting composite patterns (Diedhiou 1998). For this reason, we used the DJc results to define the best latitude and parameter references to perform the composite analysis.

From the filtered meridional wind component time series, category "*S*" dates are associated with maximum southerly wind and category "*N*" dates with maximum northerly wind. The dates of categories "*R*" (ridge) and "*T*" (trough) are at a half of the interval between "*S*" and "*N*", and "*N*" and "*S*" respectively. Four intermediate categories are also determined between "*S*" and "*R*", "*R*" and "*N*", "*N*" and "*T*", "*T*" and "*S*". Only the filtered signal is used to define the dates. After estimating the value of each unfiltered parameter for each category at each longitude, the mean values are computed for each latitude and/or each pressure level on all the waves for June–July and August–September, to build horizontal and/or vertical composite diagrams respectively. Then the composite patterns are averaged over the seventeen years from 1979 to 1995.

Duvel (1990) selected easterly waves with a modulation of at least 1 m s^{-1}. We used the whole filtered signal but we verified that results are similar when retaining only waves whose maximum of southerly wind or maximum of northerly wind is greater than 0.5 m s^{-1} in absolute value (in fact this threshold eliminates only 5% of the cases). We present here the results in August–September. Results for June–July and results obtained for a threshold greater than 2 m s^{-1} for more developed waves will also be discussed.

Table 1 shows the distribution of the filtered maximum southerly wind values for the three latitude axes and for different wind thresholds between 30°W and 30°E. As with the variance (see DJc), the percentages decrease eastward. More than half of the maxima are lower than 2 m s^{-1}, and less than 10% are greater than 4 m s^{-1}. This can be compared with the cases chosen by Reed et al. (1977) for their composite of the Phase III of GATE. Their mean meridional wind at 700 hPa is greater than 4 m s^{-1}. Apart from the fact that they use radiosonde data and not analysis values which tend to smooth the wind extrema, we can consider the easterly waves of GATE Phase III as highly developed waves. It is worth noting that the filtered 3–5-day signal is evident more eastward on the southern reference latitude (still 13% at 30°E) than on the northern reference latitude where it disappears east of 10°E.

Table 1 Contingency table of percentages of filtered maximum southerly wind at 700 hPa greater than 2 m s^{-1} (first row), 3 m s^{-1} (second row) and 4 m s^{-1} (third row) for longitudes between 30°W and 30°E. We used time series of daily June–September periods (122 days) for each year of the period 1979–1995. In each row the first line corresponds to the northern trajectory of the 3–5-day easterly waves (17.5°N over the ocean, 15°N over the continent), the second row to the southern trajectory of the 3–5-day easterly waves (5°N; not taken into account at 30°W), and the third row to the trajectory of the 6–9-day easterly waves (17.5°N)

	30°W (%)	20°W (%)	10°W (%)	0°W (%)	10°E (%)	20°E (%)	30°E (%)
V > 2	47	43	42	33	16	2	1
	–	47	42	43	27	26	13
	52	51	31	20	5	7	7
V > 3	23	20	17	12	3	–	–
	–	21	21	16	8	7	3
	20	23	9	2	–	–	1
V > 4	8	7	5	4	–	–	–
	–	7	7	6	2	–	–
	6	10	2	–	–	–	–

In the following sections, different composite diagrams will be shown both 3–5-day and 6–9-day easterly waves. It must be noted, as shown in DJa and DJc, that the respective mean wavelengths are different, about 3000 km for the 3–5-day waves north of the AEJ, 4500 km for the 3–5-day waves south of the AEJ, and about 5500 km for the 6–9-day waves. Moreover in the 6–9-day wave pattern, the extension of the anticyclonic circulation in the ridge is often larger than the cyclonic circulation in the trough. We present the perturbation of different parameters by the waves, that is for each of the eight categories and each pressure level or latitude, we subtract the average computed over the eight categories.

2.2 Horizontal patterns

Figure 1 presents different horizontal patterns of the 3–5-day waves for the northern and southern trajectories over land, and for the northern trajectory over the ocean: the wind field perturbation and associated streamlines at 700 hPa, the associated modulation of temperature at 850 hPa, of NCEP/NCAR rainfall and of IRD observed rainfall for land only.

The 700 hPa wind field and associated stream lines (Fig. 1a) over land depict a marked southwest-northeast tilt south of the AEJ and a southeast-northwest tilt north of the jet. This is consistent with a momentum transport downgradient, away from the jet, leading to wave growth by transfer of zonal kinetic energy to eddy kinetic energy. Over the ocean the tilt does not exist north of the jet and it is apparent only south of 10°N. This point is confirmed when computing the composite for a more limited area from 40°W to 20°W (not shown) more similar to the area considered by Reed et al. (1977). Over land the meridional extension of the wave is greater than over the ocean, and we note two circulation centres in the trough or in the ridge, one located at the latitude of reference, another one, weaker, located on the other side of the jet near the other reference latitude. Automatic classification applied to the 700 hPa wind field in DJc also showed the evidence of two centres located on the latitudes of the easterly waves tracks and confirms that the results of Fig. 1a are not biased by the use of particular reference latitudes. Over the ocean only one centre is observed, corresponding to the unique propagation track.

The horizontal patterns over land are similar to the pattern depicted by Burpee (1975) for the summer of 1974 where the reference latitude was 15°N. On the other hand, the pattern found by Reed et al. (1977) with a reference latitude at 11°N in the ITCZ only has one cyclonic centre at 700 hPa located at the reference latitude, with a marked southwest-northeast horizontal tilt south of 10°N and a less marked southeast-northwest tilt northward. To investigate this difference, NCEP/NCAR composite patterns have been computed relative to the reference latitude of 10°N. Resulting patterns over land in August–September (not shown) depicts also one circulation centre centred at 10°N with both north and south tilts. This confirms the influence of the reference latitude on the composite patterns and the necessity to choose a correct estimation of the wave track as the reference latitude. NCEP/NCAR composites have also been computed on the GATE Phase III period (NCEP/NCAR daily reanalyses are presently available from 1958) and confirm the previous results. The two tilts remain marked north and south of the jet over land, and the northern one decreases drastically over the ocean as in Fig. 1a.

Carlson (1969) and Burpee (1974) noted the existence of two circulation centres at the land surface, approximately located at our two reference latitudes, merging into one on an intermediate latitude over the ocean. The wave modulation of the wind at 925 hPa (not shown) is extended in latitude, with one centre over the ocean and a larger range over the land. The maximum of vorticity perturbation is located at 17.5°N near the latitude of the ITF (confluence area between the southerly monsoon flow and the northerly

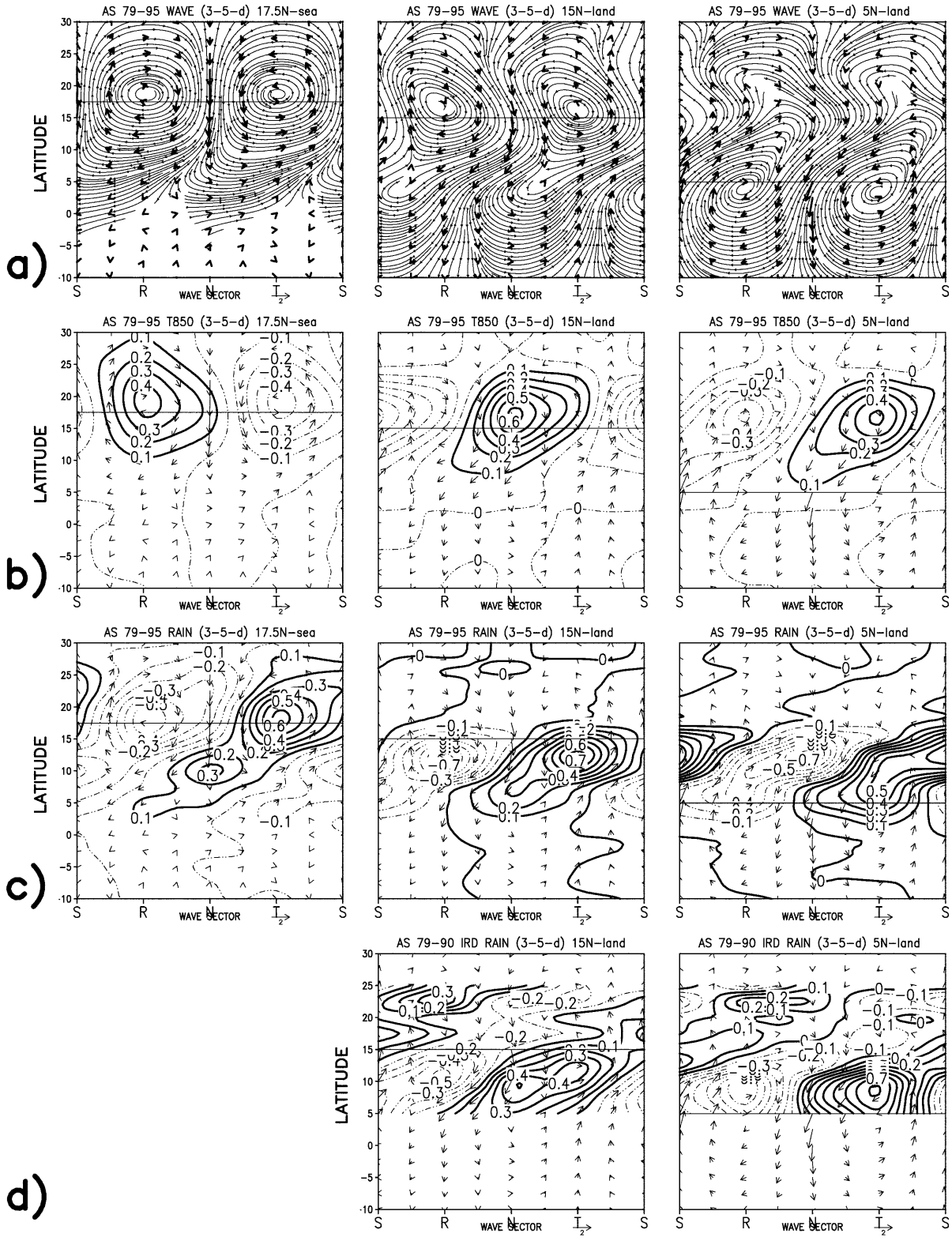

Fig. 1a–d Mean August–September 1979–95 composites computed at 700 hPa along 17.5°N over 70°W–20°W (*left*), along 15°N over 17.5°W–5°E (*middle*) and along 5°N over 17.5°W–5°E (*right*). The reference parameter is the 3–5-day filtered meridional wind at 700 hPa. **a** Modulation of wind vector and associated streamlines at 700 hPa. **b** Modulation of the temperature at 850 hPa (°C) and of 700 hPa wind vector. **c** Modulation of NCEP/NCAR rainfall (mm day^{-1}; step 0.1 mm day^{-1}) and of 700 hPa wind vector. **d** Modulation of IRD rainfall (mm day^{-1}; step 0.1 mm day^{-1}) and of 700 hPa wind vector; in this case composites are computed along 5°N over 17.5°W–5°E, and along 15°N over 17.5°W–5°E; they are averaged over the period 1979–1995 for the wind and over the period 1979–1990 for rainfall. The *vector scale* is displayed below the diagrams. The *horizontal lines* represent the latitude of reference. *S*, *R*, *N*, *T* refer to south wind, ridge, north wind, and trough sectors of the wave, respectively

Harmattan winds, where the baroclinicity is the greatest) and we also note a southward extension of the maximum of positive vorticity. This is consistent with DJc which show that the monsoon wind is modulated by the 3–5-day easterly wave with a closed circulation at 17.5°N embedded in a larger one over a broad area of West Africa. The centre of the monsoon cyclonic circulation is located in the 700 hPa wave trough sector at 5°N, ahead of the 700 hPa trough sector at 15°N, and the 700 hPa wave trough sector over the ocean.

Figure 1b shows the wave modulation of the temperature at 850 hPa. The perturbations are measured in fractions of a degree, a magnitude typical of the tropical atmosphere. Over the ocean, the largest temperature anomalies are located in the trough (cold) and in the ridge (warm) whereas over the continent, north of the AEJ, they are associated with northerly (warm) and southerly (cold) winds. Temperature anomalies at 5°N are very weak, maxima being located in the trough and the ridge (see also Fig. 3b). These anomalies are closely linked to the wind field since we note again a slight northward location of the temperature maxima relative to the reference latitudes of 15°N over the continent and 17.5°N over the ocean. The v-T covariance between wind and temperature anomalies along 15°N over the continent is negative. The consequent southward directed heat flux in a region where the temperature decreases to the south indicates that the waves are acquiring eddy available potential energy from zonal available potential energy. We will see in the following that the warm anomalies are also associated with upward velocity which can be associated with a conversion of eddy potential energy to eddy kinetic energy. The wave growth north of the AEJ can thus be explained by dry baroclinic instability. On the southern reference latitude temperature perturbations are very weak, so the wave growth cannot be understood through dry baroclinic instability. Finally over the ocean, temperature anomalies are rather high along the reference latitude but the phase quadrature between temperature and wind extrema indicates probable weaker dry baroclinic processes than over land.

Relative humidity composite patterns have also been examined (not shown). On the northern tracks, both over land and over the ocean, negative moisture anomalies are associated with northerly winds at 700 hPa, and southerly winds transport more humid air to the north. On the southern track over land, positive moisture anomalies are located in the trough and negative anomalies in the ridge.

In August–September over the land, the maximum of NCEP/NCAR rainfall wave modulation (Fig. 1c) is located in the rainbelt at about 12°N with a marked southwest extension consistent with the wave tilt at 700 hPa south of the AEJ. When considering the composite related to the reference latitude of 5°N, the maximum positive rainfall anomaly is located in the wave trough, extending to the north wind sector ahead of the trough. Northward, the maximum is located in the south wind sector where meridional advection of moist air is the largest (Burpee 1975; Reed et al. 1977; Duvel 1990). If we consider the composite related to the reference latitude at 15°N, the rainfall anomaly maximum is located in the trough at 12.5°N and is displaced to the north wind sector ahead of the trough at 5°N.

Over the ocean, the maximum positive NCEP/NCAR rainfall anomalies (Fig. 1c, left) are located in the trough on the reference latitude at 17.5°N and extends southwestward in the north wind sector ahead of the trough at 10°N. A vertical cross section of ISCCP cloud coverage along 17.5°N over the ocean (Fig. 4a) depicts positive anomalies above 700 hPa centered on the south wind sector and the anomaly range is less than half the range over the land. The pattern of rainfall anomalies over the ocean is not consistent with that of ISCCP and we are not currently enable to explain this.

Figure 1d shows similar composite rainfall patterns over the land only, computed with the observed IRD daily rain gauge measurements for the period 1979–1990. The maximum positive rainfall anomalies are also centred in the wave trough between 5°N and 10°N in the ITCZ, with a marked southwest-northeast tilt, especially for the 15°N composite. Values are greater for the reference latitude at 5°N since it is nearer the ITCZ than the northern latitude. NCEP/NCAR rainfall anomalies are in good agreement with the observed IRD anomalies. Finally rainfall patterns in June–July are similar with a slightly greater anomalies at 5°N and a slightly lower anomalies at 15°N, consistent with a more southward location of the rainbelt.

Similar patterns for the 6–9-day easterly waves are presented in Fig. 2. Let us recall that first, their mean wavelength is about 5500 km instead of 3000 km for the 3–5-day easterly waves travelling north of the AEJ, second the extension of the anticyclonic circulation in the ridge is larger than the cyclonic one in the trough (DJa, DJc). These patterns will be compared to the 3–5-day wave patterns related to the northern trajectories (15°N over land and 17.5°N over the ocean).

Figure 2 presents the horizontal patterns for the 6–9-day waves along the 17.5°N trajectories over land and over the ocean. The 700 hPa wind field and associated stream lines (Fig. 2a) shows rather similar patterns over land and over the ocean with a limited meridional extension, located mainly north of 10°N, inducing a large modulation of the zonal component of the AEJ. No tilt is evident over the land and a well-defined tilt oriented southeast-northwest is present over the ocean, north of the AEJ, suggesting a barotropic conversion of energy from the jet to the wave. In June–July the difference between land and ocean patterns is weaker since the tilt exists over the land, and also over the ocean but weaker than in August–September.

Both over land and ocean, the circulation centres are located at 20°N, that is 2.5° further north than the track defined by the kinematic analysis (DJc). The modulation of the 700 hPa geopotential height is in geostrophic balance with the wind modulation with greater signal over the ocean (not shown). It is interesting to note the opposite evolution of the two regimes of easterly waves over the land and over the ocean north of the AEJ. For the 3–5-day easterly waves, the tilt is present over land but not over the ocean. The contrary situation occurs for the 6–9-day waves. The geopotential modulation is also about twice as strong for the 6–9-day regime as for the 3–5-day regime, in accordance with the larger anticyclonic circulations observed in the 6–9-day regime (DJa, DJc).

The 925 hPa wind and its associated relative vorticity are also modulated by the wave at 700 hPa (not shown) but contrary to the 3–5-day regime, the meridional extension of this modulation is limited at 15°N over land. Over the ocean where the 6–9-day waves are more developed, the monsoon modulation extends southward to about 10°N. The maximum of vorticity modulation at 925 hPa is located at 20°N and the monsoon trough is located in the trough sector of the wave at 700 hPa. These results confirm those presented in DJc where composites were computed relative to a single point at 0°W.

The composite patterns of the temperature modulation (Fig. 2b) are similar to those associated with the 3–5-day waves along the northern track, showing positive (negative) anomalies in the north (south) wind sector over land, and in the ridge (trough) over the ocean. Compared to the 3–5-day waves, anomalies are weaker over land but stronger over the ocean. Relative humidity patterns (not shown) are also similar to the 3–5-day ones, with negative anomalies in the north wind sector and positive anomalies in the south wind sector. The anomaly range is about the same over land but twice as large over the ocean.

Over land, in the ITCZ, the NCEP/NCAR rainfall modulation (Fig. 2c), contrary to the 3–5-day easterly waves, is not linked to the trough and ridge axes but to the meridional components of the wind, northerly dry winds being associated with rainfall decrease and moist southerly monsoon winds by enhanced precipitation. Positive rainfall anomalies in the ITCZ are mainly located behind the trough, instead of in and ahead of the trough as in the 3–5-day waves. Another point of difference is that in the 3–5-day waves, rainfall anomalies are meridionaly extended in a northeast-southwest tilt (see Fig. 1c), whereas for the 6–9-day waves, anomalies are more zonally extended. This difference is actually larger than shown in the composite diagrams since the 6–9-day wavelength is almost twice as great as the 3–5-day wavelength. The fact that the 6–9-day waves have are longer and are limited north of 10°N whereas the 3–5-day waves extend more southward explains the different rainfall patterns in the ITCZ. In the 6–9-day wave regime,

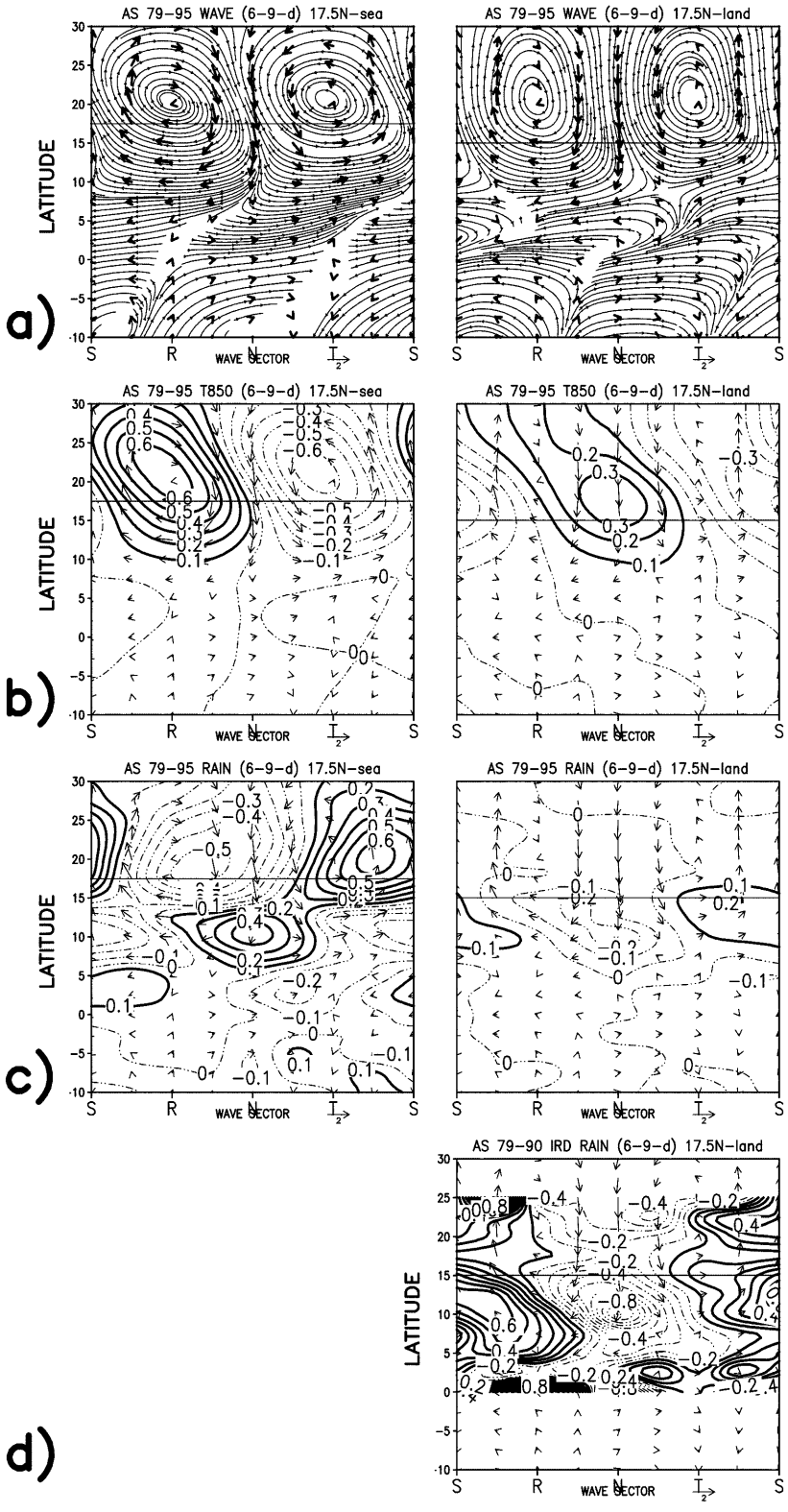

Fig. 2a–d As in Fig. 1 but for the 6–9-day easterly wave, along 17.5°N from 70°W–20°W (*left*), and 17.5°N from 17.5°W–30°E (*right*)

rainfall is enhanced mainly by the southerly winds behind the trough and also by the convergence in the zonal wind component of the AEJ. Moisture advection is therefore fundamental for rainfall production in this regime. The raw rainfall anomalies appear weaker for the 6–9-day wave composite. This is due to the fact that we computed the composite over the longitudes 17.5°W–30°E instead of 17.5°W–5°E as for the 3–5-day composite.

Over the ocean, the NCEP/NCAR rainfall modulation (Fig. 2c, left) shows positive anomalies located between the trough and the south wind sector at 20°N, and extends southwestward in the north wind sector at 10°N. This pattern is very similar to the corresponding pattern in the 3–5-day wave composite when considering the repartition of anomalies in the different wave sectors, but not consistent with ISCCP cloud coverage values at 10°N (Fig. 6b, left).

Figure 2d shows similar composite rainfall patterns over the land computed with the observed IRD daily raingauge measurements on the period 1979–1990. The maximum of positive anomalies, located in the ITCZ, are also centered in the south wind sector of the wave at 700 hPa, behind the trough. This is opposite to the rainfall modulation associated to the 3–5-day waves. The values are greater than for the NCEP/NCAR rainfall anomalies, in part because composite have been computed from the coast to 30°E in the reanalysis and to 25°E in the IRD data set, and in part because the mean NCEP/NCAR rainfall values are underestimated in the eastern part of the continental domain (DJc). However, for the repartition in the different wave sectors, the NCEP/NCAR rainfall anomalies are in good agreement with the observed IRD anomalies. Rainfall patterns in June–July are very similar with weaker anomalies at 10°N and northward, consistent with a more southward location of the rainbelt. This is due to the fact that the 6–9-day waves modulate the atmosphere mostly at and north of the AEJ latitude.

2.3 Vertical patterns

Figure 3 shows vertical cross sections in August–September of the modulation of the meridional wind component, temperature and vertical velocity by the mean composite 3–5-day easterly wave. These diagrams are shown over the ocean for the trajectory at 17.5°N (left), and over the land for the northern trajectory at 15°N (middle) and for the southern trajectory at 5°N (right). Figure 3 also presents the modulation of vertical velocity along 10°N over the continent and the ocean. Figure 4 presents similar vertical cross sections for ISCCP cloud coverage.

2.3.1 Latitude 15°N over land

The vertical profile of the meridional wind (Fig. 3a, middle) at 15°N over the land shows an eastward tilt with height below the AEJ level at 600 hPa, and a westward tilt above the jet. These slopes are in the opposite direction to the shear of the mean zonal wind. Related to the meridional gradient of temperature and its reversal at the jet level, the "*v*" profile is consistent with a jet-induced wave by baroclinic conversion of zonal available potential energy to eddy available potential energy, as shown by Burpee (1974, 1975). In the northern wind sector, the wind is northerly in the whole layer from 1000 hPa to 200 hPa, and values greater than 1 m s^{-1} are present from 950 hPa to 500 hPa. We can only note very weak positive values between 200 hPa and 100 hPa. In June–July these positive values do not exist. The same composite computed on filtered maximum meridional winds greater than 2 m s^{-1} do not show any larger reversal of sign at 200 hPa. So, contrary to the similar pattern related to the Phase III of GATE at 11°N (Reed et al. 1977), the easterly waves do not interact sufficiently strongly with convection in the north wind sector at 15°N to lead to a large opposite phase wind modulation at 200 hPa. This point is confirmed by vertical velocity and ISCCP patterns.

The vertical composite of the temperature modulation (Fig. 3b) at 15°N shows marked anomalies below the jet level, with positive values in the northerly wind advecting warm air masses from the desert and negative values in the moist cooler monsoon southerly winds. The negative *v*-*T* covariances combined with the mean positive meridional temperature gradient indicate that the wave grows by differential horizontal advection of temperature below the jet and baroclinic conversions of zonal available potential energy to eddy available potential energy.

The corresponding modulation of the vertical velocity (Fig. 3c) at 15°N shows a maximum of upward wind at 850 hPa in the north wind sector ahead and in the trough, related to convergence ahead of the trough below 800 hPa (not shown). Upward motions are also present in the trough and in the south wind sectors above the jet. Subsiding anomalies are present in the south wind and ridge sectors below the jet and in the north wind and ridge sectors above the jet level. The wave trough is thus the only sector where the deep convection is present in the whole troposphere. In June–July (not shown), the upward velocity maximum is slightly greater at 850 hPa, but above the jet level positive and negative anomalies are weaker, meaning that during this period the dry convection is enhanced in the wave but the deep convection is weakened. Diagrams for meridional winds greater than 2 m s^{-1} at 700 hPa shows a similar pattern with a quasi-doubling of the vertical velocity anomalies at 850 hPa and an increase of 50% above the jet level. There are still subsidence anomalies in the north wind sector above the AEJ. This vertical velocity pattern looks like the pattern obtained with the quasi-geostrophic theory applied to a cyclonic vorticity at the jet level in the case of dry dynamics (see Fig. 11 of Thorncroft and Hoskins 1994), with upward motions in the north wind sector below the jet and in the south wind sector above the jet, and subsiding motions in the north wind sector above the jet and in the south wind sector below the jet. The main difference between this theorical pattern and the observed one is the evidence of upward velocities in the trough sector in the whole troposphere, indicating the influence of deep convection. A computation of *w*-*T* covariances (not shown) below the jet level show a growth of the wave by baroclinic conversions of eddy potential energy to eddy kinetic energy.

The vertical profile of the relative humidity (not shown) at 15°N shows maxima in the layer 700–600 hPa up to 60%, and minima at 900 hPa (50%) and at 450 hPa (25%). The wave modulation leads to less moisture in the north wind and the trough sectors in the whole troposphere. Vertical velocity also has an impact on humidity. For instance in the north wind sector, the moisture minima at 900 hPa extend upward to 650 hPa whereas the minima at 450 hPa extend downward to 600 hPa, in agreement with the sign of the vertical velocity.

The ISCCP cloud coverage modulation patterns in August–September are presented in Fig. 4 (values are similar but slightly weaker in June–July; not shown). Cloud coverage is expressed in percent of cloudy samples in each 2.5° grid square at each atmospheric layer. In the ITCZ the mean maximum of coverage is about 12–15%. Duvel (1990) found that cloudiness below 700 hPa must be considered with care. At 15°N over land (Fig. 4a, middle), the largest positive anomalies are located in the upper troposphere between the trough and the south wind sectors. This is consistent with the modulation of the vertical velocity showing upward motions in the trough throughout the troposphere and in the south wind sector above 600 hPa. This is also consistent with the rainfall anomalies at this latitude and to the north (Fig. 1c, d). In the north wind sector, the cloud coverage anomalies are negative in the whole troposphere, and rainfall anomalies are also negative. This confirms that high values of upward motion in the north wind sector below the jet level corresponds to dry convection.

2.3.2 Latitude 5°N over land

The composite patterns at 5°N have somewhat different profiles. The axis of maximum northerly winds has less marked tilts, but the zero isolines tilt eastward with height below 900 hPa, westward between 900 hPa and 600 hPa, and eastward above, in phase with the shear of the mean zonal wind, which depicts baroclinicity opposed to the wave growth. Another difference is the evidence of weak southerly winds at 200 hPa. Associated vorticity patterns (not shown) display vertical opposition between cyclonic circulation at 700 hPa and anticyclonic circulation at 200 hPa. This is confirmed when considering composite waves where the wind modulation at 700 hPa is greater than 2 m s^{-1} (not shown). Positive values at 200 hPa in the north wind sector of the wave increase to $+0.8$ m s^{-1} and vorticity values increase too. This modulation increases to $+1.2$ m s^{-1} if we a compute composite vertical profile along 10°N in the ITCZ (not shown). This upper level wind modulation is greater in August–September than in June–July. These characteristics are consistent with a larger impact of deep convection and diabatic heating in the wave dynamics (Reed et al. 1977 for GATE Phase III; Thorncroft and Hoskins 1994).

The composite pattern of vertical velocity at 5°N (Fig. 3c, right) is somewhat different from the pattern at 15°N. Below the jet,

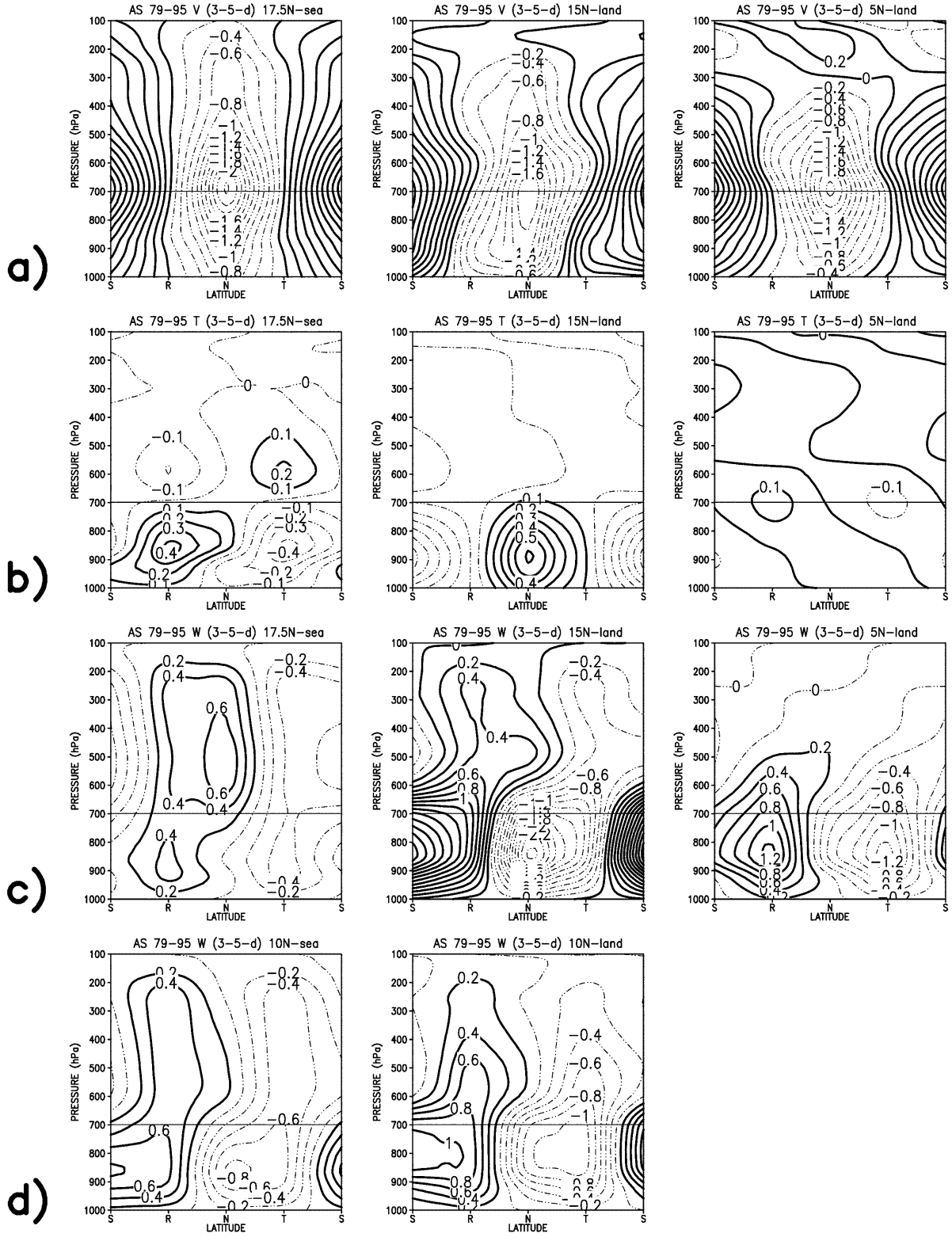

Fig. 3a–d Mean August–September 1979–95 composites of vertical cross sections along 17.5°N from 70°W–20°W (*left*), along 15°N from 17.5°W–5°E (*middle*) and 5°N from 17.5°W–5°E (*right*). The reference parameter is the 3–5-day filtered meridional wind at 700 hPa. **a** Modulation of meridional wind component (m s^{-1}). **b** Modulation of temperature (°C). **c** Modulation of vertical velocity (10^{-2} Pa s^{-1}). **d** Modulation of vertical velocity (10^{-2} Pa s^{-1}) along 10°N from 70°W–20°W (*left*) and from 17.5°W–5°E (*right*). The *horizontal line* represents the pressure level of reference. *S*, *R*, *N*, *T* refer to south wind, ridge, north wind, and trough sectors of the wave, respectively

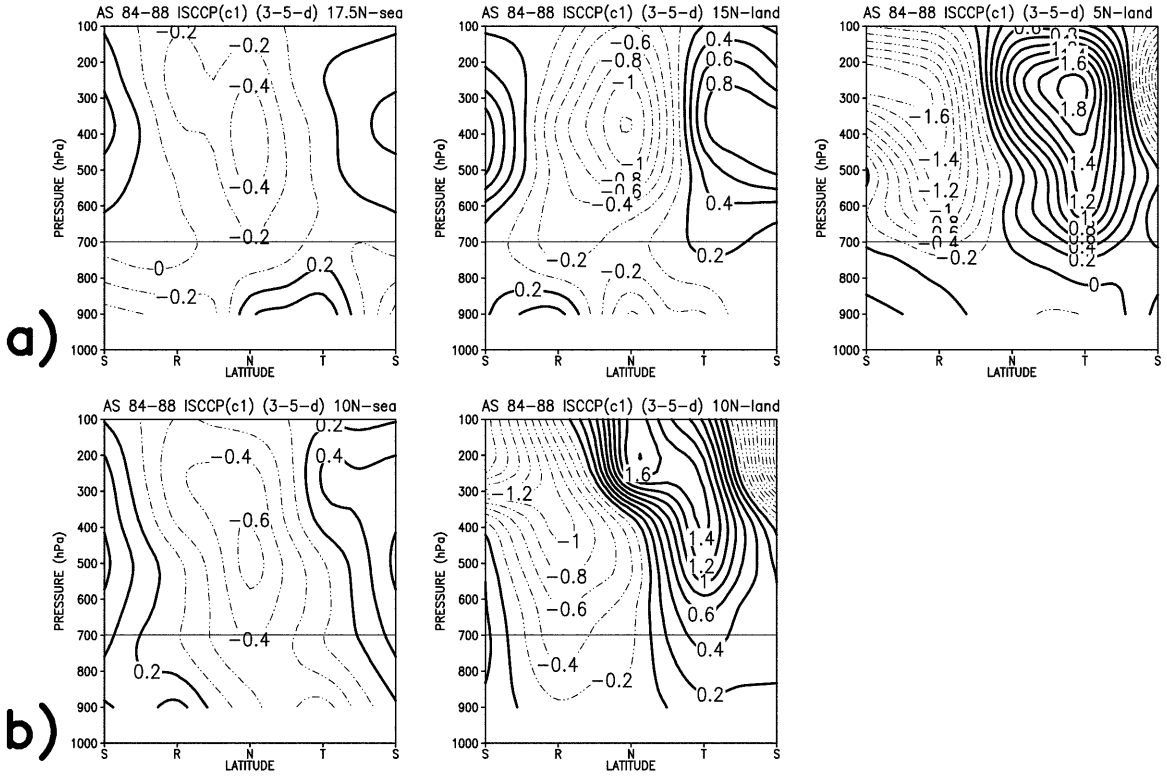

Fig. 4 a Mean August–September 1984–88 composites of vertical cross sections along 17.5°N from 70°W–20°W (*left*), along 15°N from 17.5°W–5°E (*middle*) and along 5°N from 17.5°W–5°E (*right*) of the modulation of ISCCP cloud coverage (% of cloudy pixels for each atmospheric layer in each 2.5° grid square). The reference parameter is the 3–5-day filtered meridional wind at 700 hPa. **b** as in **a** but along 10°N from 70°W–20°W (*left*) and from 17.5°W–5°E (*right*). The *horizontal line* represents the pressure level of reference. *S*, *R*, *N*, *T* refer to south wind, ridge, north wind, and trough sectors of the wave, respectively

values are weaker and the maximum of convection is now displaced eastward in the trough sector. However upward motions are still present in the north wind sector below the jet level and they replace the subsidence seen at 15°N above the jet level. In more developed waves (meridional wind greater than 2 m s^{-1}), upward motions are stronger from 900 hPa to 500 hPa with greater convergence in the trough below 900 hPa (not shown). The vertical velocities are associated with weak temperature anomalies (Fig. 3b, right). This means that the wave dynamics cannot be understood through dry baroclinic processes associated with the *v*-*T* and *w*-*T* covariances, but rather by deep convection forcing vertical motions through latent heat release. Positive relative humidity anomalies are located in the trough and negative anomalies in the ridge (not shown). The ISCCP cloud coverage modulation (Fig. 4a, right) shows large positive anomalies in the trough and north wind sectors in the middle and high troposphere, in agreement with modulation of vertical velocity and rainfall. Values are about twice as large as at 15°N due to the proximity of the ITCZ. In June–July the ISCCP anomalies are greater, due to the more southward location of the ITCZ. This is consistent with the evidence of a weak upward vertical velocity modulation in the trough sector above 400 hPa in June–July (not shown) instead of weak downward values in August–September.

We computed the composite vertical velocities and ISCCP values at 10°N in the ITCZ (Figs. 3d, Fig. 4b, middle column). The modulation of the vertical motions over land is slightly enhanced in the trough sector where the convection penetrates more in the upper troposphere. However, subsiding anomalies are still evident above 600 hPa in the north wind sector with values intermediate to those observed at 5°N and 15°N. At this latitude the deep convection is more concentrated in the trough sector. The cloud coverage modulations show positive anomalies located in and ahead of the trough in the higher levels of the troposphere.

2.3.3 Latitude 17.5°N over the ocean

The composite patterns over the ocean at 17.5°N (Fig. 3a, left) show a barotropic vertical structure for the meridional wind with no tilt anywhere in the troposphere and no reserval sign of the wind at 200 hPa, meaning no significant effect of baroclinicity. A weak tilt is present at 200 hPa for the more developed waves (wind modulation at 700 hPa greater than 2 m s^{-1}) but not strong enough to reverse the sign of the meridional wind component (a similar conclusion can be drawn for the vertical profile of vorticity). The meridional wind modulation at 700 hPa is stronger over the ocean than over land at 15°N.

The temperature perturbation at 17.5°N over the ocean (Fig. 3b, left) is well marked with lower values below the jet at 850 hPa and higher temperatures at the jet level (600 hPa) in the trough sector (the profile is reversed in the ridge), consistent with the well-know cold trough of the waves. The vorticity extrema are located at 700 hPa (not shown). The phase quadrature between *v* and *T* fields implies that the *v*-*T* baroclinic processes are weaker than at 15°N over land.

The pattern of vertical velocity at 17.5°N over the ocean (Fig. 3c, left) is also different and it is consistent with the corresponding ISCCP modulation (Fig. 4a, left). Below the jet, the upward velocity anomalies are weaker over the ocean than over land, due to less dry convection and also, less deep moist convection. The anomalies are located between the north and the south wind sectors. Above the jet, the convection is displaced towards the south wind sector. This pattern is somewhat enhanced for waves with meridional wind modulation greater than 2 m s^{-1} at 700 hPa. Baroclinic processes related to the *w*-*T* covariance show an effect of the convection opposite to the wave growth below the jet, but some positive contribution to the wave growth at the jet level (600 hPa). Moisture is the greatest in the trough sector below 850 hPa and in

the south wind sector, upward to 450 hPa (not shown), where the upward velocity is also greatest.

Convection in the ITCZ at 10°N over the ocean (Figs. 3d, Fig. 4b, left) is slightly weaker than over the land. The vertical velocity modulation depicts a maximum of upward motions in the north wind and trough sectors below the jet, and in the trough sector above the jet. The positive cloud coverage anomalies (not shown) are more concentrated in the south wind sector and they are not consistent with the rainfall anomaly pattern which shows positive anomalies in the north wind sector.

Similar patterns for the 6–9-day easterly waves are presented in Figs. 5 and 6. These patterns will be compared to the 3–5-day wave patterns related to the northern trajectories (15°N over land and 17.5°N over the ocean).

Comparing the patterns of the 6–9-day easterly waves at 17.5°N over land and ocean for the vertical profiles of meridional wind, temperature and vertical velocity modulations (Fig. 5), to the preceding patterns related to the 3–5-day easterly waves (Fig. 3) on the northern trajectories over land (15°N) and over the ocean (17.5°N), shows a close similarity. However, over land the vertical tilt of the meridional wind is weaker for the 6–9-day waves, implying weaker baroclinicity. The modulation of the convection is weaker both at 17.5°N and at 10°N in the ITCZ, as the temperature modulation at 17.5°N. For more developed 6–9-day waves (modulation of meridional wind at 700 hPa greater than 2 m s^{-1}; not shown), the vertical tilt is more evident with an eastward orientation below the jet and a westward orientation above the jet, implying stronger baroclinic processes. The convection is enhanced both below the jet in the north wind sector and above the jet in the trough sector. Over the ocean, the patterns are also very similar to the 3–5-day case but the anomalies are slightly stronger for the 6–9-day composite wave.

Over land, the cloud coverage modulation patterns (Fig. 6) confirm the difference in rainfall modulation seen before between the two easterly wave regimes. Both at 10°N in the ITCZ and at 17.5°N, the deep convection is located behind the trough in the 6–9-day wave composite whereas it is located at and ahead of the trough in the ITCZ for the 3–5-day wave composite. Since the vertical velocity patterns do not show a similar variation, we can conclude that rainfall and convection are more sensitive to the horizontal transport of moisture in the 6–9-day wave regime. Over the ocean, the cloud coverage pattern is similar to the 3–5-day patterns, except in the lower layers where the positive anomalies extend from the south wind sector to the trough sector at 17.5°N. At the reference latitude of 10°N, the maximum of cloud coverage is also located behind the trough, and it is not consistent with the NCEP/NCAR rainfall modulation.

3 General synthesis

It was shown in DJa and DJc that the 6–9-day easterly wave regime over West Africa and the tropical Atlantic could be interpreted as an interaction between the classical 3–5-day easterly wave regime, linked to the barotropic–baroclinic instability of the AEJ, and the development of strong anticyclones north of the jet, in the areas of the Azores and the Libyan highs. DJc also showed that over West Africa, rainfall in the ITCZ and the monsoon flux are modulated differently by the two wave regimes. To explore this question further, we have analysed horizontal and vertical composite patterns of the two easterly wave regimes separately over land and ocean.

The results obtained with the NCEP/NCAR reanalyses over the period 1979–1995, confirm the previous results based on smaller samples. These easterly waves grow over West Africa west of 20°E and move westwards over the tropical Atlantic.

The 3–5-day easterly waves modulate the wind field over the whole of West Africa. An automatic classification (DJc) showed that over land, about one third of the waves have typically two circulation centres on the two tracks (5°N and 15°N), the other two thirds have one circulation centre located over one of the two tracks. Consequently the modulation of the monsoon winds by the easterly waves are more extended over land, in agreement with results of Carlson (1969), Burpee (1974) and DJc. The waves are tilted along a southeast-northwest direction north of the AEJ and along a southwest-northeast direction south of the jet. Along the northern trajectory deep convection interacts with these waves but mostly trough horizontal transport of moisture, leading to most convective clouds in and behind the wave trough in the south wind sector. Along the southern trajectory, in the ITCZ, the easterly waves also interact positively with the deep convection, upward motions being located in and ahead of the trough, increasing cyclonic vorticity by the vertical stretching effect.

Over the ocean, the two trajectories merge into one, along 15–20°N, the southern one following the northwest-southeast oriented line of the meridional PV gradient on the southern edge of the AEJ. West of 30°W, the easterly waves have a clear cold core below the jet level and they are maintained mainly by barotropic energy conversions. Upward motions in the cold core of the wave could act on the wave decay below the jet level. Above the jet level these upward velocities are mainly located in and behind the trough, but cloud coverage maxima are mostly located in the south wind sector. The convection is weaker and seems to be less sensitive to the horizontal moisture advection than over the land since this factor is not as limiting as over the Sahelo-Saharan band.

The 3–5-day easterly wave circulation is greater in August–September than in June–July both over land and ocean. Over land the temperature contrasts and the dry convection modulation north of 15°N are stronger in June–July. Finally the northward excursion of the ITCZ between June–July and August–September leads to a stronger deep convection modulation by the wave at 5°N in June–July and at 15°N in August–September.

The results obtained for the 6–9-day easterly waves confirm the occurrence of such a synoptic regime growing north of the AEJ. We have shown in DJa and DJc that the anticyclonic circulations located in the wave ridge are larger in this 6–9-day regime, with a greater wavelength and a resulting period. This point has not been simply restated in this work, because here we work on composite diagrams in which the wavelength information is omitted. However, composite patterns over the tropical Atlantic still show larger modulations of temperature, geopotential height and cloud coverage, as well as a more marked horizontal tilt even if these wave modulations appear weaker over land. The overall composite patterns for the 6–9-day wave

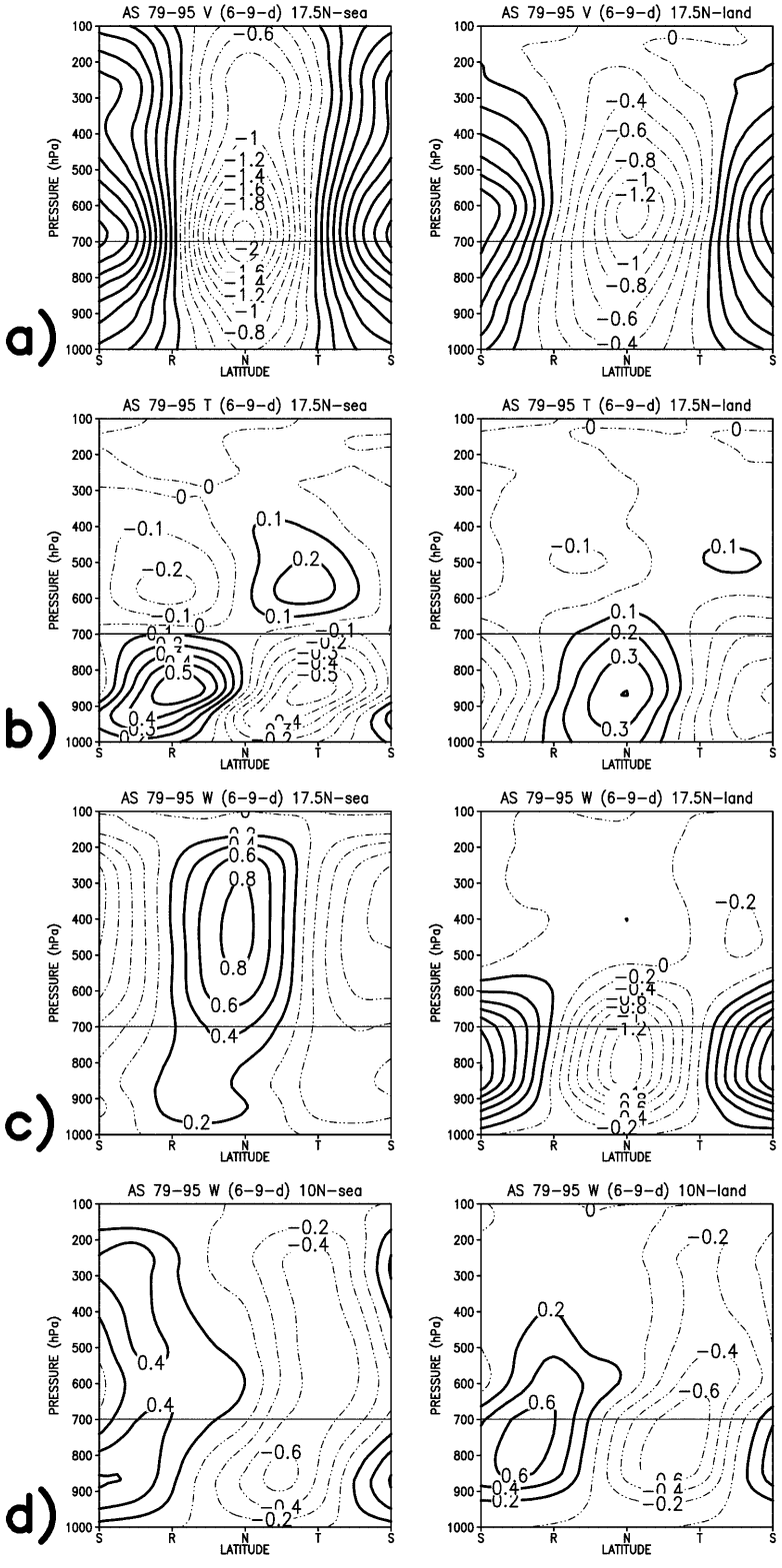

Fig. 5 a, **b**, **c** As in Fig. 3–c but for the 6–9-day easterly wave, along 17.5°N from 70°W–20°W (*left*), and along 17.5°N from 17.5°W–30°E (*right*). **d** As in Fig. 3d but for the 6–9-day easterly wave, along 10°N from 70°W–20°W (*left*) and from 17.5°W–30°E (*right*)

regime are similar to those related to the 3–5-day wave regime. However we note some significant differences.

The 6–9-day waves travel in a more northward direction and are less meridionaly extended over land. These waves are associated with a strong modulation of the zonal wind component of the AEJ. Positive rainfall anomalies are mainly located in the south wind sector behind the trough, both in the ITCZ (in contrast with the 3–5-day waves) and over the Sahelo-Saharan band (as for the 3–5-day waves). The 6–9-day rainfall

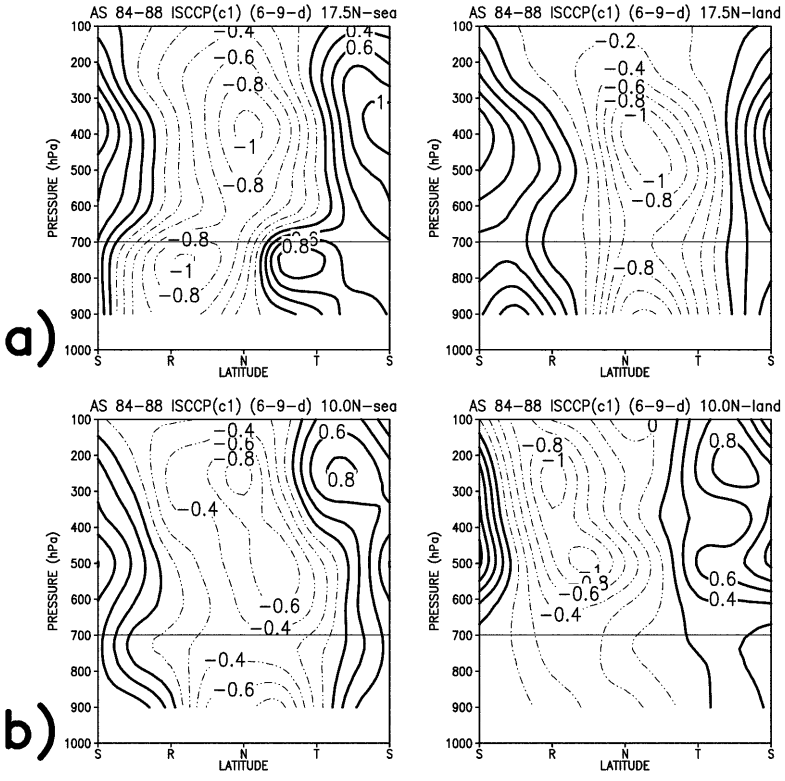

Fig. 6 **a** As in Fig. 4a but for the 6–9-day easterly wave, along 17.5°N from 70°W–20°W (*left*), and along 17.5°N from 17.5°W–30°E (*right*). **b** As in Fig. 4b but for the 6–9-day easterly wave, along 10°N from 70°W–20°W (*left*) and from 17.5°W–30°E (*right*)

modulation seems to be controled mainly by the horizontal transport of moisture over the Sahelo-Saharan band and also by the zonal moisture convergence in the AEJ. This leads to a more elongated rainfall bands (DJc).

We note from Fig. 6 that the ISCCP cloud coverage modulation is similar over land and over the ocean, whereas the 3–5-day modulation is larger over land where the upward motion forcing on cloud coverage is stronger. This point confirms the more important role of zonal moisture transport and the relative unimportance of vertical velocities for 6–9-day cloud coverage modulation, and it is in accordance with the preferential location of clouds in the south wind sector behind the trough. We also note that in the ITCZ over land, the 3–5-day cloud modulation is about twice as large as for the 6–9-day modulation, but the rainfall modulation is similar. Over the ocean at 17.5°N, the cloud modulation is twice as large for the 6–9-day waves and slightly greater at 10°N.

The stronger modulation of the 6–9-day waves over the ocean, relative to the 3–5-day waves, is also evident in the geopotential heights and the temperature fields, and it can be associated with the stronger developed anticyclonic circulations already pointed out in DJa and DJc. It could also correspond to a larger barotropic energy conversion since a marked southeast-northwest tilt is evident north of the AEJ whereas it is missing for the 3–5-day waves. On the other hand, the 6–9-day waves are somewhat less developed over land, consistent with their weaker barotropic and baroclinic patterns compared to the 3–5-day wave regime.

The main sign of the seasonality in the 6–9-day wave activity is the increase of the rainfall modulation in August–September when the ITCZ is further north. The fact that this wave pattern is limited mostly north of the AEJ latitude leads to a weaker ITCZ rainfall modulation in June–July.

A 17-year climatology of the main terms in the energy equations relative to these wave regimes has to be made to estimate the relative contribution of barotropic and baroclinic energy transfers following Reed et al. (1988), and to verify the hypotheses suggested here for the maintenance of these waves over land and ocean.

We have also shown that rainfall and convection are modulated in a different way over West Africa by the 6–9-day regime. It may be interesting to look at the characteristics of rainfall events associated with this synoptic regime (mesoscale convective complexes, monsoon rains), as well as their frequency of occurrence and their persistence, and to consider the possible differences with the 3–5-day synoptic regime.

The onset of the 6–9-day wave regime and its dissipation should be investigated further, both with reanalysis data and modelling sensitivity experiments to test the relative roles of the anticyclonic centres of action in the Libyan and Azores areas, the land surface energy exchanges in the heat low, and the subtropical westerly jet. The question of why this regime is statistically identified in the 6–9-day band-period (i.e. why the wavelength is around 5000 km and the phase speed around 7 m s^{-1}; see DJc) also merits further investigation.

Acknowledgements The authors are very grateful to Climate Diagnostics Center (NOAA, Boulder, CO) for providing the NCEP/NCAR Reanalysis dataset, to Abraham H. Oort for providing the "GFDL Atmospheric Circulation Tape Library 1958–1989" and to Thierry Lebel and Henri Laurent for providing IRD daily rainfall dataset. The authors also thank Jean Louis Monge for his efficiency in managing the CLIMSERV database at LMD and Laurence Picon for her help in reading ISCCP data. Final thanks to Brian Doty for the availability of the graphics software GrADS, Claire Guilhot, Christian Velpry for their help and to Nick Hall for corrections to English and comments. This work was partly supported by the European Contract WAMP (West African Monsoon Project) no ENV4-CT97-0500.

References

Burpee RW (1974) Characteristics of North African easterly waves during the summers of 1968 and 1969. J Atmos Sci 31: 1556–1570

Burpee RW (1975) Some features of synoptic-scale waves based on a compositing analysis of GATE data. Mon Weather Rev 103: 921–925

Carlson TN (1969) Some remarks on African disturbances and their progress over the tropical Atlantic. Mon Weather Rev 97: 716–726

Chen YL, Ogura Y (1982) Modulation of convective activity by large-scale flow pattern observed during GATE. J Atmos Sci 39: 1260–1279

Diedhiou A (1998) Easterly wave regimes over West Africa and the tropical Atlantic. Thesis of University Paris 12, pp 230 (in French)

Diedhiou A, Janicot S, Viltard A, de Félice P (1998a) Evidence of two regimes of easterly waves over West Africa and the tropical Atlantic. Geophys Res Let 25: 2805–2808

Diedhiou A, Janicot S, Viltard A, de Félice P, Laurent H (1998b) A fast eastern waves in West Africa troposphere. Meteorol Atmos Phys 69: 39–47

Diedhiou A, Janicot S, Viltard A, de Félice P, Laurent H (1999) Easterly waves regimes and associated convection over West Africa and the tropical Atlantic: results from the NCEP/NCAR and ECMWF reanalyses. Clim Dyn 15: 795–822

Duvel JP (1990) Convection over tropical Africa and the Atlantic ocean during northern summer. Part II: modulations by easterly waves. Mon Weather Rev 118: 1855–1868

Reed RJ, Recker EE (1971) Structures and properties of synoptic-scale wave disturbances in the equatorial western Pacific. J Atmos Sci 28: 1117–1133

Reed RJ, Norquist DC, Recker EE (1977) The structure and properties of African wave disturbances as observed during Phase III of GATE. Mon Weather Rev 105: 317–333

Reed RJ, Klinder E, Hollingsworth A (1988) The structure and characteristics of African easterly wave disturbances determined from ECMWF operational analysis/forecast system. Meteorol Atmos Phys 38: 22–33

Rossow WB, Schiffer RA (1991) ISCCP cloud data products. Bull Am Meteorol Soc 72: 2–20

Thompson RM, Payne SW, Recker EE, Reed RJ (1979) Structure and properties of synoptic-scale wave disturbances in the intertropical convergence zone of the eastern Atlantic. J Atmos Sci 36: 53–72

Thorncroft CD, Hoskins BJ (1994a) An idealized study of African easterly waves. Part I: A linear view. Q J R Meteorol Soc 120: 953–982